# 3D phenomenological modeling of plasma-assisted methane reforming

Praise Noah Johnson\*, Taaresh Sanjeev Taneja<sup>†</sup> and Suo Yang<sup>‡</sup>

Department of Mechanical Engineering, University of Minnesota – Twin Cities, Minneapolis, MN 55455, USA

Natural gas contains a significant fraction of methane, a strong greenhouse gas besides being a potent hydrogen carrier. Thus, reforming methane to a more reactive gas mixture could potentially abate the associated greenhouse heating by depleting methane and provide a pathway to generate hydrogen. The present study investigates the non-equilibrium plasmaassisted reforming of methane to produce hydrogen and reactive alkenes using repetitive nanosecond pulse discharges. A detailed gas-phase chemical kinetics mechanism along with plasma reforming kinetics derived from our previous work are used to perform 0D calculations to obtain the energy fractions for various plasma processes. A phenomenological model for the plasma-assisted reforming of methane/nitrogen mixtures is developed by considering the vibrational energy transport equations of both methane and nitrogen separately. The energy fractions involved in various plasma processes, such as ultra-fast gas heating and ultra-fast gas dissociation due to the electron excitation reactions, and slow gas heating due to the relaxation of vibrational excitation modes of methane and nitrogen, are accounted for in our new phenomenological model using energy fractions derived earlier. The newly developed phenomenological model is then used to perform 3D direct numerical simulation (DNS) of methane reforming diluted with 60% nitrogen in a pin-to-pin electrode configuration with a discharge gap of 1 mm. The effect of pulsing on the evolution of reformed mixture kernels is investigated by comparing two cases: a single-pulsed case with a pulse energy of 0.8 mJ, and another case using 4 pulses at 200 kHz, with a per pulse energy of 0.2 mJ. The single-pulsed case was observed to promote kernel separation and higher fractions of reformed products, while the multiple-pulsed case resulted in a more diffused kernel.

## I. Nomenclature

 $u_i = i^{th}$  velocity component

 $\rho$  = gas density  $\rho$  = gas pressure

 $\tau_{ij}$  = viscous stress tensor

 $\tau_{ij}$  = viscous stress tensor  $Y_k$  = mass fraction of species k

 $V_{k,i} = i^{th}$  component of the mixture-averaged diffusion velocity of species k

 $W_k$  = molar mass of species k

 $\dot{\omega}_{k}^{c}$  = net molar production rate of species k due to combustion

H = total non-chemical enthalpy per unit mass

 $q_i$  =  $i^{th}$  component of heat flux vector  $h_s$  = sensible enthalpy per unit mass

 $\dot{Q}_{react}$  = heat release rate due to combustion reactions

 $D_{CH_4}$  = diffusion coefficient of CH<sub>4</sub>

 $\tau_{VT}$  = time-scale of vibrational-to-translational relaxation

## **II. Introduction**

METHANE (CH<sub>4</sub>), a widely available gas is among the primary constituent in natural gas mixtures [1] from petrochemical industries and is also one of the major products in various biological and physical processes [2].

<sup>\*</sup>Ph.D. Student, Student Member AIAA

<sup>†</sup>Ph.D. Candidate, Student Member AIAA.

<sup>‡</sup>Richard & Barbara Nelson Assistant Professor, suo-yang@umn.edu (Corresponding Author), Senior Member AIAA.

Though high in hydrogen content per carbon basis compared to other hydrocarbon gases, the separation of CH<sub>4</sub> from petrochemical extraction cites and its transport to distant locations for consumer utility poses economical and logistical challenges [3]. To safely discard the CH<sub>4</sub> uneconomical to extract and transport, routine activities such as venting or flaring of natural gas are often performed at the extraction sites [4]. Venting and flaring the natural gas into the atmosphere results in a considerable greenhouse effect owing to the 80 times more pronounced greenhouse effect of CH<sub>4</sub> when compared to CO<sub>2</sub> [5–7] owing to the incomplete destruction of CH<sub>4</sub> by flaring. Thus, it is paramount to explore techniques to improve CH<sub>4</sub> destruction by improving the reactivity of natural gas mixtures. Of all the different methods to improve the reactivity of natural gas, reforming of CH<sub>4</sub> to produce H<sub>2</sub> and other reactive hydrocarbons is investigated extensively [8–11]. Nevertheless, challenges exist associated with the reforming of CH<sub>4</sub> to useful products owing to a completely symmetrical tetrahedral structure and a high C-H bond energy of 438.8 kJ/mol [3]. Thus, the strong and weakly polarised C-H bond dissociation requires highly energetic reactants and extreme conditions like high pressure and temperature, which are enabled by energy-intensive processes. Therefore it is critical to explore reformation techniques that are less energy-intensive, yet capable of efficient C-H bond cleavage.

One way to enhance the cleavage of the C-H bond and formation of reactive species efficiently in the gas mixture is to perform a plasma-assisted reforming (PAR), where, the gas mixture can be reformed to a more reactive mixture by treating it with nanosecond repetitively pulsed (NRP) non-equilibrium plasma discharges [12, 13]. The application of the gas mixture with NRP discharges results in the production of electrons and ions, along with excited species [14, 15]. In addition, PAR gives rise to several reactive radicals such as H and CH<sub>3</sub> due to the proceeding of electron impact dissociation reactions involving  $CH_4$  (e<sup>-</sup> +  $CH_4$   $\longrightarrow$  e<sup>-</sup> +  $CH_x$  + (4 - x)H) as observed in our recent 0D study [16]. These reactions, along with the subsequent H-abstraction and recombination reactions result in the production of H<sub>2</sub> and reactive alkene species [16] in the natural gas mixture. Regardless of these findings from 0D investigation, practical plasma systems often involve non-plane electrode geometries like pin-to-pin configuration resulting in a spatiallydependent plasma [17]. Consequently, detailed 2D/3D plasma modeling is required to encompass the spatiotemporal effects of NRP discharges on the reforming of the gas mixture. Several modeling approaches exist varying from the high-fidelity and computationally expensive particle-in-cell/Monte Carlo collision (PIC/MCC) simulations to lesser expensive fluid-based simulations [18, 19]. Despite their availability, such methods are computationally complex and are nonviable to be used to simulate practical PAR systems involving complex chemical species. To abate the computational complexity of plasma calculations, recent studies [20-22] incorporated the prime effects of NRP discharges such as ultra-fast and slow gas heating and ultra-fast dissociation of O<sub>2</sub> from 0D calculations into 3D DNS ignition studies. As such, these studies [20–22] observed the development of an ignition kernel and the subsequent spatiotemporal propagation/quenching of the kernel at different conditions without directly computing the plasma kinetics. Therefore, a similar implementation of the phenomenological plasma model for PAR of CH<sub>4</sub>/N<sub>2</sub> mixtures, is therefore, considered to enable practical computations for PAR of CH<sub>4</sub>.

The aim of the present study is twofold: i) Firstly, the present study aims to extend the phenomenological NRP discharge model of Castela et al. [20] by accounting for the dissociation of  $CH_4$  to the major radicals along with fast-gas heating and vibrational energy transport, followed by ii) investigating the formation and propagation of the reformation kernel in a  $CH_4/N_2$  mixture and the influence the pulsed discharges over a single pulse discharge. The present article is organized as follows: Section III discusses the numerical methodology and the phenomenological plasma-assisted  $CH_4$  reforming model used to simulate the PAR of  $CH_4/N_2$  mixtures. The numerical results of  $CH_4$  reforming and the effects of different conditions are presented in Sec. IV, following which, the conclusions are summarized in Sec. V.

## III. Methodology

#### A. Numerical methodology

A quarter section of the pin-to-pin geometry in a cylindrical domain of radius 8 mm and length 5 mm as shown in Fig. 1 is used in the present work. A gap distance of 1 mm is maintained at the center of the domain and the pin-pin electrode geometry is considered in mesh generation. The mesh contains 18.18 million cells with the smallest cell size of 5  $\mu$ m (along the radial direction) at the discharge center, and a maximum cell size of 35  $\mu$ m at the boundaries in the radial direction. Along the axial direction, the cell size varies between 6  $\mu$ m near the electrodes to 33  $\mu$ m at the boundary. The outflow boundaries of the cylinder are maintained using wave transmissive boundary conditions to permit the propagation of the reforming kernel without being reflected back. Second-order, total variation diminishing central difference schemes were used for the gradient, divergence, and Laplacian terms of all the governing equations.

The temperature is fixed to 300 K everywhere and the calculations are performed at atmospheric pressure. The

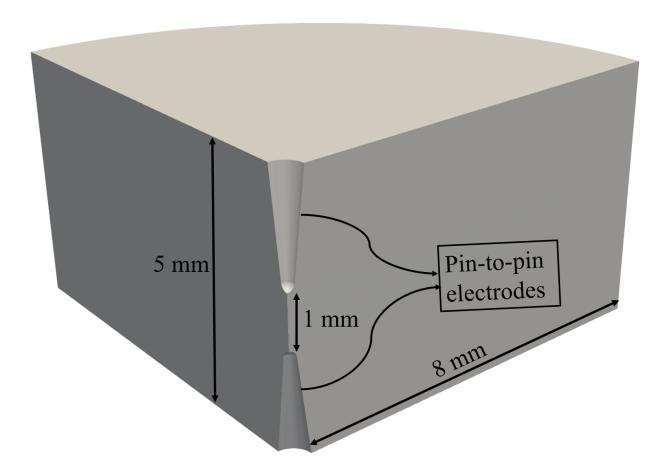


Fig. 1 The computational domain used for numerical calculations in the present work.

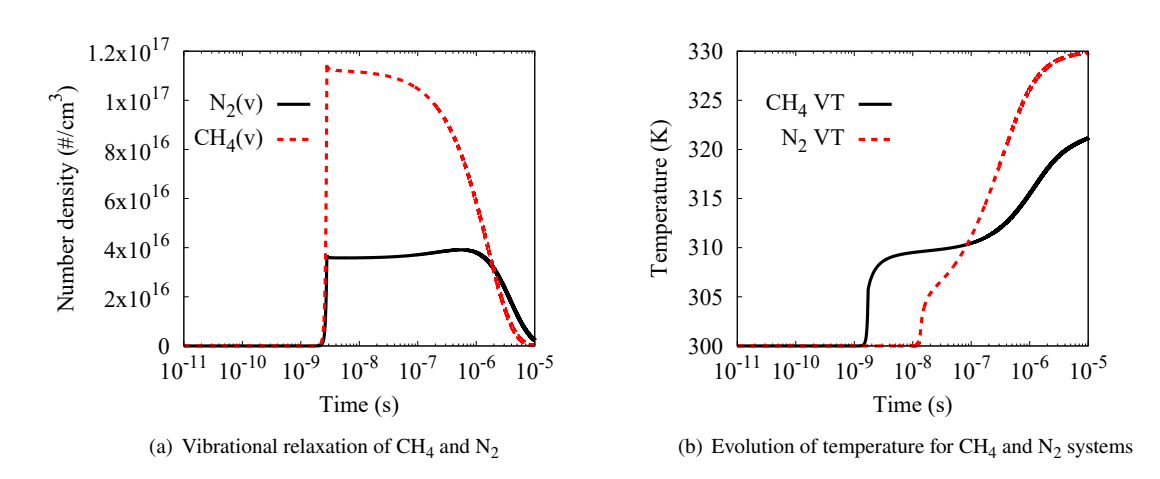


Fig. 2 Evolution of (a) the number densities of  $N_2(v)$  and  $CH_4(v)$ , along with (b) the temperature evolution due to vibrational-translational (VT) relaxation for a discharge in pure  $CH_4$  and  $N_2$ .

gas-phase chemistry model used for methane reforming is a reduced version of the GRI mechanism [23] containing 30 species and 184 reactions. For the NRP discharges, the pulse width is fixed to 20 ns, and the time step is fixed to 0.5 ns during the pulses and is allowed to vary in the gap based on the CFL number.

#### B. Reformation kinetics and PAR model

The phenomenological NRP plasma ignition model proposed by Castella et al. [20] has been adapted in the present work to model plasma-assisted reforming (PAR) of  $CH_4/N_2$  mixtures. The model discussed herein has been implemented in-house [21, 22] on the OpenFOAM [24] platform. When the NRP discharges are characterized by a reduced electric field (E/N) ranging from 100 to 400 Td (1 Td =  $10^{-17}Vcm^2$ ), about 90% of the deposited pulse energy  $\dot{E}_p$  is found to be stored in vibrational and electronic modes of  $CH_4$  and  $N_2$ . The vibrational excitation of  $CH_4$  and  $N_2$  occurs in a few 10's of nanoseconds and the corresponding de-excitation occurs in much longer microsecond time scales as seen in Fig. 2(a) The number densities of vibrationally excited  $CH_4$  ( $CH_4(v)$ ) is found to be significant ( $\sim$  3 times higher) when compared to that of  $N_2$  ( $N_2$ (v)). Moreover, the relaxation of  $CH_4(v)$  is found to happen significantly earlier when compared to  $N_2$ (v). Similar observations can be made from the temperature rise due to the vibrational-translational (VT) relaxations as shown in Fig. 2(b), where the early temperature rise due to VT relaxation ( $< 1 \times 10^{-7}$  s) of  $CH_4(v)$  is higher compared to that of  $N_2$ (v). Post  $1 \times 10^{-7}$  s, the contribution of VT relaxation of  $CN_2$ (v) dominates as observed in Fig. 2(b). To account for these complexities in VT relaxation in the  $CH_4/N_2$  gas mixture, it is essential to accommodate the vibrational energy transport due to both  $CH_4$  and  $N_2$ . Thus, the two-step phenomena of slow gas heating due to the

vibrational energy transport can then be depicted by:

*Ultrafast vibrational energy increase*:  $CH_4/N_2 + e^- \longrightarrow CH_4(v)/N_2(v) + e^-$ ;

Slow heating by VT relaxation: 
$$CH_4(v)/N_2(v) + X \longrightarrow CH_4/N_2 + X + Heat$$
,

where  $CH_4(v)$  and  $N_2(v)$  represents a general vibrational state of  $CH_4$  and  $N_2$  respectively and X being any species. Unlike vibrational relaxation, the electronic excitation of  $CH_4$  and  $N_2$  and subsequent dissociation of  $CH_4$  to radicals occur in a few 10's nanoseconds, thereby resulting in ultrafast dissociation of  $CH_4$  and ultrafast gas heating as shown by the following reaction:

Ultrafast heating and dissociation:  $CH_4 + e^- \longrightarrow CH_4(e) + e^- \longrightarrow CH_x + (4 - x)H + e^- + Heat$ 

Ultrafast heating and dissociation via 
$$N_2(e)$$
:  $CH_4 + N_2(e) \longrightarrow CH_x + (4 - x)H + N_2 + Heat$ 

where,  $N_2(e)$  and  $CH_4(e)$  represents a general electronic excited state of  $N_2$  and  $CH_4$  respectively.

Thus, the energy deposited in the pulse  $\dot{E}_p$  is divided into three components contributing to ultrafast gas heating  $(\dot{E}_{p,heat})$ , ultrafast CH<sub>4</sub> dissociation  $(\dot{E}_{p,diss})$ , and ultrafast increase in the vibrational energy of the gas  $(\dot{E}_{p,vib})$ , in addition to electron kinetic energy  $(\dot{E}_{p,elec})$  as given by Eq. 1:

$$\dot{E}_p = \dot{E}_{p,heat} + \dot{E}_{p,diss} + \dot{E}_{p,vib} + \dot{E}_{p,elec} \tag{1}$$

In Eq. 5,  $\dot{E}_{p,vib}$  is comprised of the vibrational energy contributions from both CH<sub>4</sub> ( $\dot{E}_{p,vib,CH_4}$ ) and N<sub>2</sub> ( $\dot{E}_{p,vib,N2}$ ), such that  $\dot{E}_{p,vib} = \dot{E}_{p,vib,CH_4} + \dot{E}_{p,vib,N2}$ . The set of equations solved by accounting for the three major effects of NRP discharges in CH<sub>4</sub> reforming is then given below:

$$\frac{\partial \rho}{\partial t} + \frac{\partial (\rho u_i)}{\partial x_i} = 0 \tag{2}$$

$$\frac{\partial(\rho u_j)}{\partial t} + \frac{\partial(\rho u_i u_j)}{\partial x_i} = -\frac{\partial p}{\partial x_j} + \frac{\partial \tau_{ij}}{\partial x_i}$$
 (3)

$$\frac{\partial(\rho Y_k)}{\partial t} + \frac{\partial(\rho u_i Y_k)}{\partial x_i} = -\frac{\partial}{\partial x_i} (\rho V_{k,i} Y_k) + W_k \dot{\omega}_k^c + + W_k \dot{\omega}_k^p$$
(4)

$$\frac{\partial(\rho H)}{\partial t} + \frac{\partial(\rho u_i H)}{\partial x_i} = -\frac{\partial q_i}{\partial x_j} + \frac{\partial(\tau_{ij} u_i)}{\partial x_i} + \frac{\partial p}{\partial t} - \frac{\partial}{\partial x_i} \left(\rho \sum_{k=1}^{N_{sp}} h_{s,k} Y_k V_{k,i}\right) + \dot{Q}_{react} + \dot{E}_{p,heat} + \dot{R}_{VT,CH_4}^p + \dot{R}_{VT,N_2}^p$$
 (5)

Eqs. 2, 3, 4, and 5 represent the continuity, momentum, species, and energy conservation equations with appropriate additional source terms to accommodate the effects of plasma. In Eq. 4,  $\dot{\omega}_k^P$  ( $\dot{\omega}_{CH_4}^P$ ,  $\dot{\omega}_{CH_3}^P$ ,  $\dot{\omega}_{CH_2}^P$ , and  $\dot{\omega}_H^P$  in this study) denotes the molar production rate to model the production of species by ultra-fast dissociation of gas species (CH<sub>4</sub> in the present work). In Eq. 5, H denotes the total non-chemical enthalpy per unit mass and is given by  $h_s + \frac{1}{2}u_iu_i$ . The slow gas heating due to VT relaxation of CH<sub>4</sub>(v) and N<sub>2</sub>(v) is accounted for by adding vibrational energy relaxation rates for CH<sub>4</sub>(v) and N<sub>2</sub>(v) ( $\dot{R}_{VT,CH_4}^P$  and  $\dot{R}_{VT,N_2}^P$ ) to the energy equation (see Eq. 5). In order to balance the vibrational energy  $\dot{E}_{p,vib}$  and the corresponding VT relaxation rates  $\dot{R}_{VT,CH_4}^P$  and  $\dot{R}_{VT,N_2}^P$ , two additional conservation equations (see Eq. 6 and 7) for the specific vibrational energy carried by CH<sub>4</sub> ( $e_{vib,CH_4}$ ) and N<sub>2</sub> molecules ( $e_{vib,N_2}$ ) are added to the system of equations:

$$\frac{\partial(\rho e_{vib,CH_4})}{\partial t} + \frac{\partial(\rho u_i e_{vib,CH_4})}{\partial x_i} = -\frac{\partial}{\partial x_i} \left(\rho D_{CH_4} \frac{\partial e_{vib,CH_4}}{\partial x_i}\right) + \dot{E}_{p,vib,CH_4} - \dot{R}_{VT,CH_4}^p \tag{6}$$

$$\frac{\partial(\rho e_{vib,N_2})}{\partial t} + \frac{\partial(\rho u_i e_{vib,N_2})}{\partial x_i} = -\frac{\partial}{\partial x_i} \left(\rho D_{N_2} \frac{\partial e_{vib,N_2}}{\partial x_i}\right) + \dot{E}_{p,vib,N_2} - \dot{R}_{VT,N_2}^p \tag{7}$$

To close this model, we assume a fractions  $\alpha$ ,  $\beta_k$  for the  $k^{th}$  dissociation product of CH<sub>4</sub> ( $\beta_H$ ,  $\beta_{CH_2}$ , and  $\beta_{CH_3}$  in the present study), and  $\gamma_j$  for the  $j^{th}$  species contributing towards vibrational energy of the system ( $\gamma_{CH_4}$  and  $\gamma_{N_2}$  in

this study). An additional fraction  $\eta$  is also considered to account for the kinetic energy of electrons. Thus the energy deposited by the pulse  $\dot{E}_p$  can then be distributed into four parts:

$$\dot{E}_p = \alpha \dot{E}_p + \sum_k \beta_k \dot{E}_p + \sum_j \gamma_j \dot{E}_p + \eta \dot{E}_p \tag{8}$$

The fractions  $\beta_k$  and  $\gamma_j$  can be directly obtained using 0D calculations, where,  $\beta_k$  corresponding to the  $k^{th}$  radical can be calculated using:

$$\beta_k = \frac{N_k \Delta H_k^\#}{E_{P,0D}} \tag{9}$$

$$\gamma_j = \frac{N_j E_{th,j}}{E_{p,0D}} \tag{10}$$

In Eq. 9,  $N_k$  denotes the number density (cm<sup>-3</sup>) of the  $k^{th}$  dissociation product,  $\Delta H_k^{\#}$  denotes the formation enthalpy in J/molecule for k, and  $E_{p,0D}$  represents the energy deposited in the 0D calculations (J/cm<sup>3</sup>). A similar approach could be utilized to calculate the fractions  $\gamma_j$  for the  $j^{th}$  species contributing to the vibrational energy increase of the system, with  $\Delta H^{\#}$  replaced by the threshold energy ( $E_{th,j}$ ) for the vibrational excitation of j (J/molecule) as shown in Eq. 10. The fraction  $\eta$  can also be obtained from the 0D calculation by utilizing the expression for electron kinetic energy as given in literature [25]. Now, fraction of energy for fast-gas heating  $\alpha$  can be simply calculated using:

$$\alpha = 1 - \sum_{k} \beta_k - \sum_{j} \gamma_j - \eta \tag{11}$$

These fractions  $\alpha$  and  $\gamma_j$  can now be utilized to calculate  $\dot{E}_{p,heat}$ ,  $\dot{E}_{p,vib,CH_4}$ , and  $\dot{E}_{p,vib,N_2}$ . To calculate the species production source terms in Eq. 4,  $\dot{E}_{p,diss}$  can be expressed as:

$$\dot{E}_{p,diss} = g_{diss}\dot{E}_{p},\tag{12}$$

where  $g_{diss}$  denotes the fraction of  $\dot{E}_p$  used for ultra-fast dissociation. If  $h_{f,k}$  is the specific formation enthalpy of the species k, then  $\dot{E}_{p,diss}$  can also be given by

$$\dot{E}_{p,diss} = \sum_{k=1}^{N_{sp}} h_{f,k} \dot{\omega}_k^p = \sum_{k=1}^{N_{sp}} g_{diss}^k \dot{E}_p, \tag{13}$$

where,  $g_{diss}^k$  denotes the fraction of  $\dot{E}_p$  expend to produce species k. Therefore, the species production rate by plasma  $\dot{\omega}_k^p$  for a species k is given by Eq. 14.  $g_{diss}^k$  is assumed to be proportional to  $\frac{Y_{CH_4}}{Y_{CH_4}^f}$  where  $Y_{CH_4}^f$  is the mass fraction of CH<sub>4</sub> in the fresh mixture. If  $\beta_k$  is the fraction of  $\dot{E}_p$  leading to CH<sub>4</sub> dissociation,  $g_{diss}^k$  can then be written as given in Eq. 15.

$$\dot{\omega}_k^P = g_{diss}^k \frac{\dot{E}_p}{h_{f,k}};\tag{14}$$

$$g_{diss}^{k} = \beta_{k} \frac{Y_{CH_{4}}}{Y_{CH_{4}}^{f}}.$$
 (15)

Since the present work considers the dissociation of CH<sub>4</sub> to H, CH<sub>3</sub>, and CH<sub>2</sub>, the conservation of mass involving plasma reactions give

$$\dot{\omega}_{CH_4}^p = -\left(\dot{\omega}_{CH_3}^p + \dot{\omega}_{CH_2}^p + \dot{\omega}_H^p\right) = -\frac{Y_{CH_4}\dot{E}_p}{Y_{CH_4}^f} \left(\frac{\beta_{CH_3}}{h_{f,CH_3}} + \frac{\beta_{CH_2}}{h_{f,CH_2}} + \frac{\beta_H}{h_{f,H}}\right). \tag{16}$$

In Eq. 5 6, and 7,  $\dot{R}^p_{VT,j}$  for the  $j^{th}$  species is calculated using the Landau-Teller harmonic oscillator approach as given by

$$\dot{R}_{VT,j}^{p} = \rho \frac{e_{vib,j} - e_{vib,j}^{eq}(T)}{\tau_{VT,j}}$$
 (17)

where  $e_{vib,j}^{eq}(T)$  denotes the equilibrium vibrational energy of the  $j^{th}$  species at a given temperature T and is given by:

$$e_{vib,j}^{eq}(T) = \frac{r_j \Theta_{1,j}}{e^{\frac{\Theta_{1,j}}{T}} - 1},$$
(18)

where  $\Theta_{1,j}$  is the vibrational temperature of the  $j^{th}$  species corresponding to its first quantum vibrational state and  $r_j = \frac{R_u}{W_j} (R_u \text{ being the universal gas constant})$ . The present study utilizes  $\Theta_{1,N_2} = 3396 \text{ K}$  [20] and  $\Theta_{1,CH_4} = 1880 \text{ K}$  [26]. In Eq. 17,  $\tau_{VT,j}$  is given by:

$$\tau_{VT,j} = \left(\sum_{M} \frac{1}{\tau_{VT,j}^{M}}\right)^{-1},\tag{19}$$

where M denotes the collisional partners of j. The relaxation times  $\tau_{VT,CH_4}$  and  $\tau_{VT,N_2}$  are calculated from the rate coefficients in the literature [27] as stated elsewhere [28].

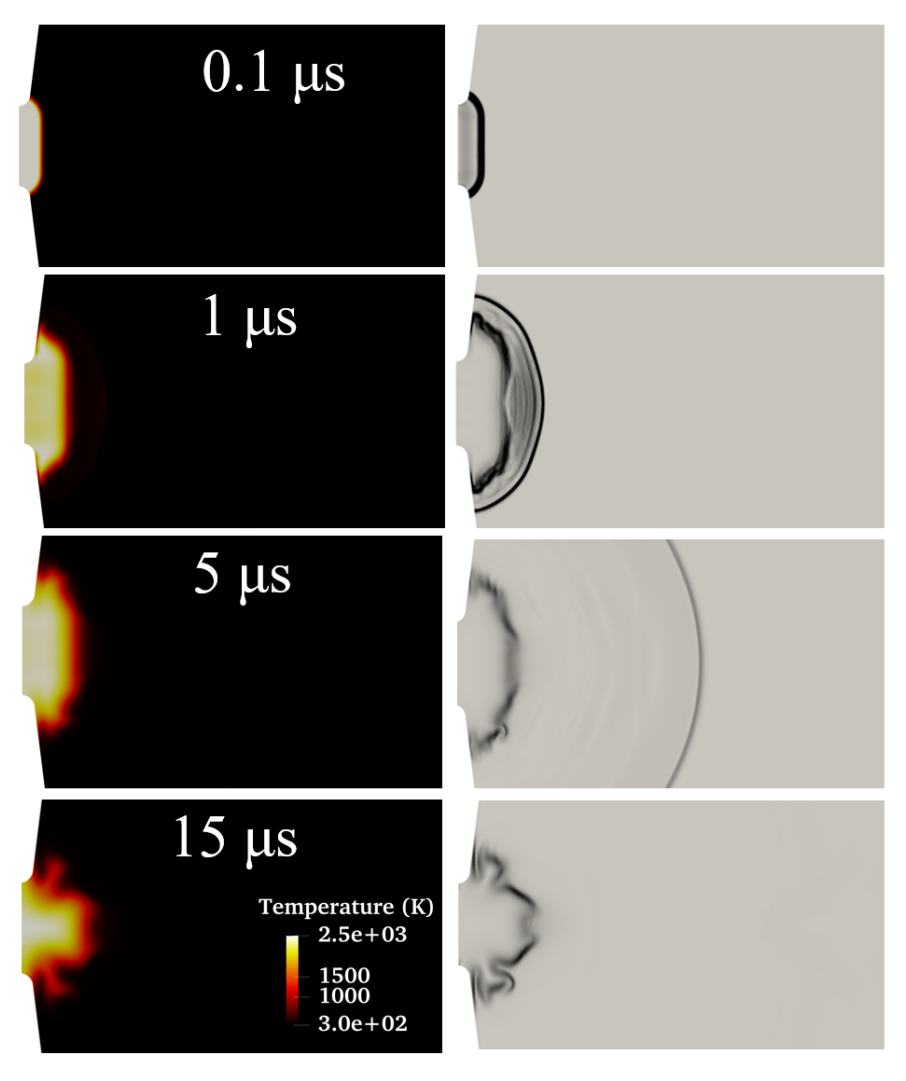


Fig. 3 Evolution of temperature and density gradient (i.e., numerical schlieren) at different time instances after the discharge pulse.

# IV. Results and Discussion

An in-house 0D NRP discharge code [25] is utilized to perform 0D plasma discharges in a  $CH_4/N_2$  mixture at 300 K and atmospheric pressure using a recently derived detailed plasma reforming mechanism for small alkanes [16]. The

simulations are performed for a single pulse, with the pulse energy fixed to  $0.05 \text{ J/cm}^3$  and a reduced electric field (E/N) of 200 Td (1 Td =  $10^{-17} \text{ V cm}^2$ ). This value of E/N corresponds to an applied voltage of 4.8 kV in a pin-to-pin setup with a gap distance of 1 mm. The fractions obtained from the 0D calculations are shown in Table 1 and will be utilized for subsequent PAR computations.

Table 1 Energy fractions for various plasma effects obtained using 0D modeling of PAR of CH<sub>4</sub>/N<sub>2</sub> mixtures.

$\beta_{CH_3}$	$eta_{CH_2}$	$\beta_H$	$\gamma_{CH_4}$	$\gamma_{N_2}$	η
0.0532	0.0479	0.1565	0.0903	0.0885	0.06

## A. Evolution of the reforming core

The phenomenological model introduced in the present study is utilized to simulate a single discharge of non-equilibrium plasma in CH<sub>4</sub>, diluted with 40% N<sub>2</sub>. The pulse energy is set to 0.8 mJ and the plasma energy fractions shown in Table 1 are used to account for various effects of plasma discharge. Fig. 3 shows the evolution of temperature and the gradient of density post-discharge for various instances. It can be observed that the temperature peaks around  $\sim$  2500 K at 0.1  $\mu$ s, and the hot core is limited within the electrode gap with a cylindrical shape. As time progresses, the

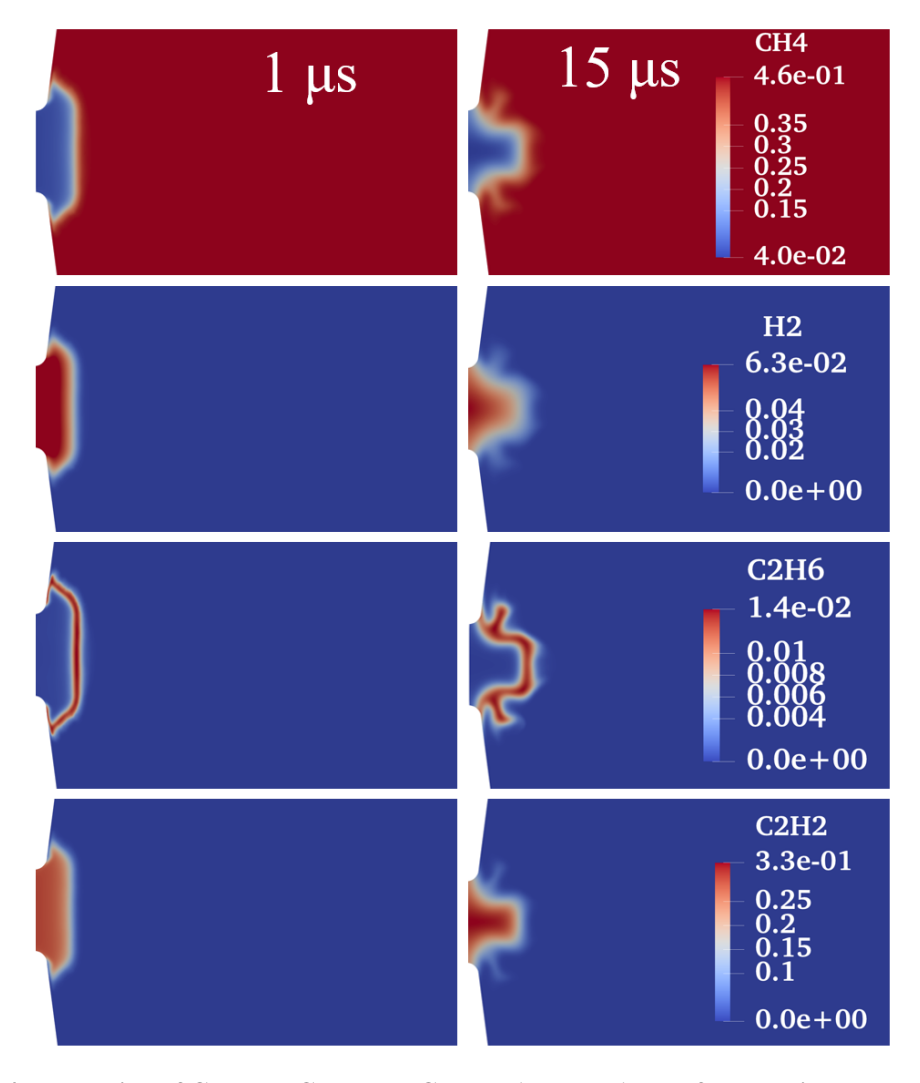


Fig. 4 Evolution of CH<sub>4</sub>, H<sub>2</sub>, C<sub>2</sub>H<sub>6</sub>, and C<sub>2</sub>H<sub>2</sub> at 1  $\mu$ s and 15  $\mu$ s after the discharge pulse.

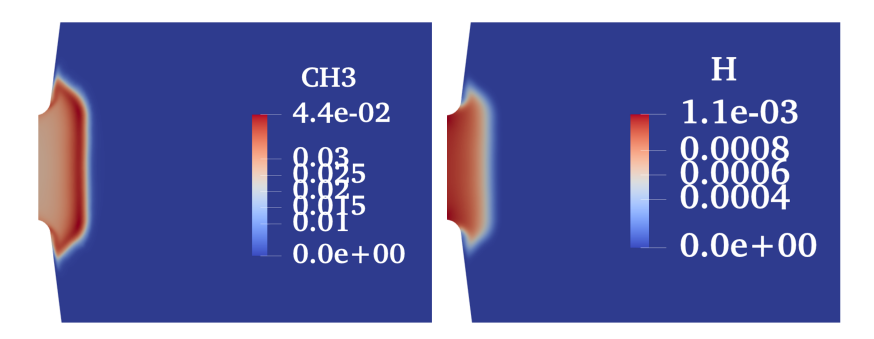


Fig. 5 Contours of CH<sub>3</sub> and H at 1  $\mu$ s after the discharge pulse.

hot core proceeds to expand outside the gap, with the hot kernel moving around the electrode tip, and further at 15  $\mu$ s, the cylindrical kernel collapses to form a toroidal kernel. Similar observations can be found from the evolution of the density gradient. Fig. 4 portrays the evolution of CH<sub>4</sub>, along with the different reformed products such as H<sub>2</sub>, C<sub>2</sub>H<sub>6</sub>, and C<sub>2</sub>H<sub>2</sub> for two different instances. The discharge gap is found to be significantly CH<sub>4</sub>-depleted, whereas, the same region is found to be occupied with reformed H<sub>2</sub> and C<sub>2</sub>H<sub>2</sub> (see Fig. 4). Despite the production of H<sub>2</sub> and C<sub>2</sub>H<sub>2</sub>, the hot (reforming) kernel did not accommodate the production of C<sub>2</sub>H<sub>6</sub> (see Fig. 4) and C<sub>2</sub>H<sub>4</sub>. The production of the aforementioned species were, however, limited to the thin outer region of the reforming kernel at all time instances. To better understand the accumulation of C<sub>2</sub>H<sub>6</sub> and C<sub>2</sub>H<sub>4</sub> at the kernel boundaries, the contours of CH<sub>3</sub> and H are shown in Fig. 5, which depicts an accumulation of CH<sub>3</sub> and depletion of H at the kernel boundaries. The accumulated CH<sub>3</sub> proceed to recombine and form C<sub>2</sub>H<sub>6</sub> as the temperature in the outer region is in the range between 700-1300 K. When compared to the kernel boundary, the hot core of the reforming kernel maintains a significantly higher temperature (~ 2500 K), thereby dissociating any recombined C<sub>2</sub>H<sub>6</sub> and C<sub>2</sub>H<sub>4</sub>. In contrast, C<sub>2</sub>H<sub>2</sub> contains a strong C- C triple bond in comparison to C<sub>2</sub>H<sub>4</sub> and C<sub>2</sub>H<sub>6</sub>. In addition, higher temperature facilitates multiple C-H bond scissions thereby promoting an increased presence of H and CH radicals, whereas, CH<sub>3</sub> and CH<sub>2</sub> are reduced. This is evident from Fig. 5, where the hot core is found to contain lesser CH<sub>3</sub> and more H radicals as compared to the kernel boundary.

#### B. Effect of multiple pulses on reforming

To understand the effect of multiple pulses on reformed product evolution, the phenomenological model was utilized to simulate NRP discharges in  $CH_4/N_2$  mixtures at a repetition frequency of 200 kHz. The number of pulses was limited to four with the energy per pulse set to 0.2 mJ to match the total energy deposition in the single-pulse discharge presented earlier. Figure 6 shows the contours of  $C_2H_4$  and  $H_2$  at 20  $\mu$ s after the last plasma discharge. It can be observed that the reforming kernel in the single-pulse case (on the left in Fig. 6) proceeds to eject radially outwards with a decreased thickness of the preceding hot core, betraying a subsequent separation of the reforming kernel to form a toroidal structure. However, the 4-pulse case tends to have a more diffuse reforming core with the kernel boundaries attaching to the outer electrode regions. Thus unlike the single-pulse case, the 4-pulse case does not tend toward a toroidal separation. Moreover, the mass fractions of  $C_2H_4$  - a clear indicator of the reforming kernel boundary as per the previous discussion - are observed to be comparatively lower for the 4-pulsed case. This suggests a more diffused core region, which could be a consequence of the pulse energy distributed across four pulses, thereby leading to a diffused plasma.

Since the energy deposited in each pulse in the 4-pulse scenario is lower by a factor of 4, the  $CH_4$  decomposition and the temperatures are also found to be significantly lower for the 4-pulse case immediately after the first pulse (around 2% of  $CH_4$  is decomposed) in comparison to the single-pulse scenario where about 80% of the  $CH_4$  in the discharge gap is found to be decomposed. Nevertheless, around 0.1-1  $\mu$ s, the former is found to have much higher temperatures (around 4000 K), despite the energy per pulse being lower by a factor of 4. This can be attributed to the pronounced presence of  $CH_4$  molecules after the first pulse (in the 4-pulse case) compared to the single-pulse case. The presence  $CH_4$  introduces an early VT relaxation in times lesser than  $10^{-7}$  s, whereas, the VT relaxation in the single pulse case comes into effect only at a later time (after  $10^{-7}$  s). The difference in VT time scales between  $CH_4$  and  $N_2$  can be observed in Fig. 2. The effect of early VT relaxation on the kernel evolution in the 4-pulse case and the effect of subsequent heating due to the VT relaxation of  $N_2$  is unresolved at the time of submission of this manuscript. More information on the interplay between VT relaxation timescales of  $CH_4$  and  $N_2$  and their effect on the reforming kernel evolution will be discussed in

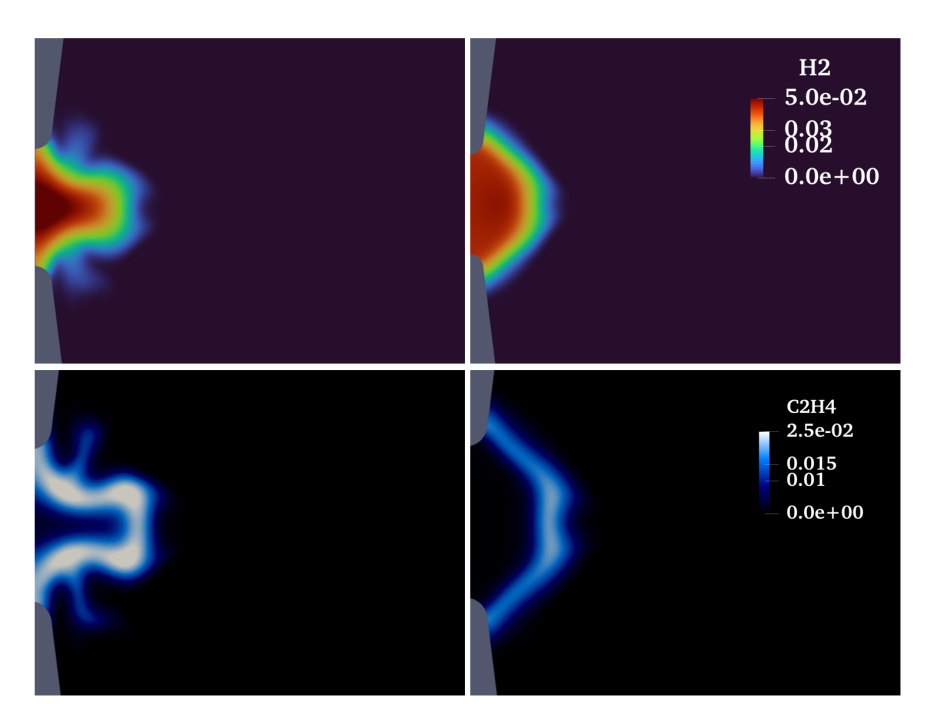


Fig. 6 Contours of  $C_2H_4$  and  $H_2$  for the single-pulse discharge (left) and the 4-pulse discharge (right) at 20  $\mu$ s after the discharges.

the future.

# V. Conclusion

A phenomenological model to simulate the nanosecond repetitively pulsed (NRP) plasma-assisted reforming (PAR) of  $CH_4/N_2$  mixtures is developed in the present work based on plasma-assisted combustion (PAC) models available in the literature [20, 22]. The model has been developed by considering energy fractions for various plasma processes: ultra-fast gas heating and  $CH_4$  dissociation due to electronic excitation, and slow gas heating due to vibrational-translational (VT) relaxation of  $CH_4$  and  $N_2$ . The vibrational energy transport was accounted for using separate transport equations of vibrational energy for both  $CH_4$  and  $N_2$ . The application of the newly developed phenomenological model to  $CH_4$  reforming in a pin-to-pin electrode configuration separated by 1 mm depicted the propagation of reforming kernel and  $H_2$  production along with other higher hydrocarbons.  $H_2$  and  $C_2H_2$  were found to occupy the discharge gap, while the accumulation of  $C_2H_6$  and  $C_2H_4$  were limited to the reforming kernel boundaries. A single discharge case with a pulse energy of 0.8 mJ was found to promote kernel separation and higher reformed fractions over the 4-pulse case with each pulse depositing 0.2 mJ, and the latter was observed to produce a diffused reaction kernel.

## Acknowledgments

The information, data, or work presented herein was funded in part by the Advanced Research Projects Agency-Energy (ARPA-E), U.S. Department of Energy, under Award Number DE-AR0001529, and in part by the National Science Foundation (NSF) under Award Number CBET 2002635. The views and opinions of authors expressed herein do not necessarily state or reflect those of the United States Government or any agency thereof. The authors also acknowledge the Minnesota Supercomputing Institute (MSI) for its computational resources.

## References

- [1] Saha, D., Grappe, H. A., Chakraborty, A., and Orkoulas, G., "Postextraction separation, on-board storage, and catalytic conversion of methane in natural gas: a review," *Chemical reviews*, Vol. 116, No. 19, 2016, pp. 11436–11499.
- [2] Segers, R., "Methane production and methane consumption: a review of processes underlying wetland methane fluxes,"

- Biogeochemistry, Vol. 41, 1998, pp. 23–51.
- [3] Sun, L., Wang, Y., Guan, N., and Li, L., "Methane activation and utilization: Current status and future challenges," *Energy Technology*, Vol. 8, No. 8, 2020, p. 1900826.
- [4] Brzustowski, T., "Flaring in the energy industry," Progress in Energy and Combustion Science, Vol. 2, No. 3, 1976, pp. 129–141.
- [5] Jain, A. K., Briegleb, B. P., Minschwaner, K., and Wuebbles, D. J., "Radiative forcings and global warming potentials of 39 greenhouse gases," *Journal of Geophysical Research: Atmospheres*, Vol. 105, No. D16, 2000, pp. 20773–20790.
- [6] Pachauri, R. K., Allen, M. R., Barros, V. R., Broome, J., Cramer, W., Christ, R., Church, J. A., Clarke, L., Dahe, Q., Dasgupta, P., et al., Climate change 2014: synthesis report. Contribution of Working Groups I, II and III to the fifth assessment report of the Intergovernmental Panel on Climate Change, Ipcc, 2014.
- [7] Ialongo, I., Stepanova, N., Hakkarainen, J., Virta, H., and Gritsenko, D., "Satellite-based estimates of nitrogen oxide and methane emissions from gas flaring and oil production activities in Sakha Republic, Russia," *Atmospheric Environment: X*, Vol. 11, 2021, p. 100114.
- [8] Barelli, L., Bidini, G., Gallorini, F., and Servili, S., "Hydrogen production through sorption-enhanced steam methane reforming and membrane technology: a review," *Energy*, Vol. 33, No. 4, 2008, pp. 554–570.
- [9] Li, D., Nakagawa, Y., and Tomishige, K., "Methane reforming to synthesis gas over Ni catalysts modified with noble metals," *Applied Catalysis A: General*, Vol. 408, No. 1-2, 2011, pp. 1–24.
- [10] Sheu, E. J., Mokheimer, E. M., and Ghoniem, A. F., "A review of solar methane reforming systems," *International Journal of Hydrogen Energy*, Vol. 40, No. 38, 2015, pp. 12929–12955.
- [11] Chen, T. Y., Taneja, T. S., Rousso, A. C., Yang, S., Kolemen, E., and Ju, Y., "Time-resolved in situ measurements and predictions of plasma-assisted methane reforming in a nanosecond-pulsed discharge," *Proceedings of the Combustion Institute*, Vol. 38, No. 4, 2021, pp. 6533–6540.
- [12] Kim, W., Mungal, M. G., and Cappelli, M. A., "The role of in situ reforming in plasma enhanced ultra lean premixed methane/air flames," *Combustion and Flame*, Vol. 157, No. 2, 2010, pp. 374–383.
- [13] Sun, W., Uddi, M., Won, S. H., Ombrello, T., Carter, C., and Ju, Y., "Kinetic effects of non-equilibrium plasma-assisted methane oxidation on diffusion flame extinction limits," *Combustion and Flame*, Vol. 159, No. 1, 2012, pp. 221–229.
- [14] Yang, S., Nagaraja, S., Sun, W., and Yang, V., "Multiscale modeling and general theory of non-equilibrium plasma-assisted ignition and combustion," *Journal of Physics D: Applied Physics*, Vol. 50, No. 43, 2017, p. 433001.
- [15] Yang, S., Gao, X., Yang, V., Sun, W., Nagaraja, S., Lefkowitz, J. K., and Ju, Y., "Nanosecond pulsed plasma activated C2H4/O2/Ar mixtures in a flow reactor," *Journal of Propulsion and Power*, Vol. 32, No. 5, 2016, pp. 1240–1252.
- [16] Johnson, P. N., Taneja, T. S., and Yang, S., "Plasma Assisted Emission Control of Hydrocarbon Gas Flares: A 0D Feasibility Study," AIAA SCITECH 2023 Forum, 2023, p. 2060.
- [17] Pai, D. Z., Stancu, G. D., Lacoste, D. A., and Laux, C. O., "Nanosecond repetitively pulsed discharges in air at atmospheric pressure—the glow regime," *Plasma Sources Science and Technology*, Vol. 18, No. 4, 2009, p. 045030.
- [18] Kim, H., Iza, F., Yang, S., Radmilović-Radjenović, M., and Lee, J., "Particle and fluid simulations of low-temperature plasma discharges: benchmarks and kinetic effects," *Journal of Physics D: Applied Physics*, Vol. 38, No. 19, 2005, p. R283.
- [19] Becker, M. M., Kählert, H., Sun, A., Bonitz, M., and Loffhagen, D., "Advanced fluid modeling and PIC/MCC simulations of low-pressure ccrf discharges," *Plasma Sources Science and Technology*, Vol. 26, No. 4, 2017, p. 044001.
- [20] Castela, M., Stepanyan, S., Fiorina, B., Coussement, A., Gicquel, O., Darabiha, N., and Laux, C. O., "A 3-D DNS and experimental study of the effect of the recirculating flow pattern inside a reactive kernel produced by nanosecond plasma discharges in a methane-air mixture," *Proceedings of the Combustion Institute*, Vol. 36, No. 3, 2017, pp. 4095–4103.
- [21] Taneja, T. S., and Yang, S., "Comparing Low-Mach and Fully-Compressible CFD Solvers for Phenomenological Modeling of Nanosecond Pulsed Plasma Discharges with and without Turbulence," AIAA Scitech 2022 Forum, 2022, p. 0976.
- [22] Taneja, T. S., Ombrello, T., Lefkowitz, J., and Yang, S., "Numerical Investigation of Ignition Kernel Development with Nanosecond Pulsed Plasma in Quiescent and Flowing Mixtures," *AIAA SCITECH 2023 Forum*, 2023, p. 0749.

- [23] Smith, G. P., Golden, D. M., Frenklach, M., Moriarty, N. W., Eiteneer, B., Goldenberg, M., Bowman, C. T., Hanson, R. K., Song, S., Gardiner Jr, W. C., et al., "GRI 3.0 Mechanism," *Gas Research Institute (http://www.me. berkeley. edu/gri\_mech)*, 1999.
- [24] Jasak, H., "OpenFOAM: open source CFD in research and industry," *International Journal of Naval Architecture and Ocean Engineering*, Vol. 1, No. 2, 2009, pp. 89–94.
- [25] Taneja, T. S., Johnson, P. N., and Yang, S., "Nanosecond pulsed plasma assisted combustion of ammonia-air mixtures: Effects on ignition delays and NOx emission," *Combustion and Flame*, Vol. 245, 2022, p. 112327.
- [26] Person, W. B., and Zerbi, G., "Vibrational intensities in infrared and Raman spectroscopy," (No Title), 1982.
- [27] Starikovskiy, A., and Aleksandrov, N., "Plasma-assisted ignition and combustion," *Progress in Energy and Combustion Science*, Vol. 39, No. 1, 2013, pp. 61–110.
- [28] Barléon, N., Cheng, L., Cuenot, B., and Vermorel, O., "A phenomenological model for plasma-assisted combustion with NRP discharges in methane-air mixtures: PACMIND," *Combustion and Flame*, Vol. 253, 2023, p. 112794.